On the incorporation of iron into hexagonal barium titanate: II. Magnetic moment, electron paramagnetic resonance (EPR) and optical transmission

OPEN ACCESS
IOP Publishing
Journal of Physics: Condensed Matter
J. Phys.: Condens. Matter **32** (2020) 385702 (8pp)
https://doi.org/10.1088/1361-648X/ab9345

On the incorporation of iron into hexagonal barium titanate: II. Magnetic moment, electron paramagnetic resonance (EPR) and optical transmission

H T Langhammer[1,3], T Walther[1], R Böttcher[2] and S G Ebbinghaus[1]

[1] Institut für Chemie, Martin-Luther-Universität Halle-Wittenberg, Kurt-Mothes-Straße 2, D-06120 Halle, Germany
[2] Fakultät für Physik und Geowissenschaften, Universität Leipzig, Linnéstraße 5, D-04103 Leipzig, Germany

E-mail: hans.langhammer@physik.uni-halle.de, till.walther@chemie.uni-halle.de, boettch@physik.uni-leipzig.de and stefan.ebbinghaus@chemie.uni-halle.de

Received 7 April 2020, revised 11 May 2020
Accepted for publication 14 May 2020
Published 19 June 2020

Abstract

Systematic measurements of the magnetic moment in dependence on temperature and magnetic field of hexagonal 6H-$BaTiO_3$ + 0.04 BaO + x/2 Fe_2O_3 ($0.005 \leqslant x \leqslant 0.05$) ceramics were performed to study the influence of Fe ions on the magnetic properties. While the samples show Curie–Weiss paramagnetism for Fe concentrations $\leqslant$1.0 mol%, antiferromagnetic interactions become manifest for 2.0 and 5.0 mol% iron. With increasing Fe content the antiferromagnetic interaction, which is assumed to be caused by a superexchange mechanism $Fe^{3+}_{Ti(1)} - O^{2-}_{O(2)} - Fe^{3+}_{Ti(2)}$, becomes stronger. At external magnetic fields smaller than 1 T a further, ferromagnetic interaction between Fe^{3+} ions is detected below 200 K. The interactions between Fe^{3+} ions in the samples with 2.0 and 5.0 mol% iron are also manifest in the EPR spectra by numerous lines with low intensity. Q-band EPR investigations of 5.0 mol% Fe doped single crystals confirm the existence of only one type of Fe^{3+}–V_O associates in the samples.

Keywords: barium titanate, iron doped, hexagonal, magnetic susceptibility, electron paramagnetic resonance, optical transmission

(Some figures may appear in colour only in the online journal)

1. Introduction

Barium titanate ($BaTiO_3$) represents a material of fundamental importance for a wide range of technical applications. It is in the focus of solid-state research for example in the context of multiferroic materials and the investigation of the new class of dilute magnetic oxides (DMOs) [1–4]. The incorporation of Fe is known to stabilize the hexagonal high-temperature phase of $BaTiO_3$ at room temperature (RT) [5]. Already rather small amounts of iron in the order of 1 mol% cause purely hexagonal 6H-$BaTiO_3$ ceramics after sintering at 1400 °C in air [6, 7]. On the other hand, the sintering conditions strongly depend on the Sr content of the samples, since already small amounts of Sr (as a common impurity in the raw material $BaCO_3$) distinctly shift the phase transition temperature cubic–hexagonal to higher temperatures [8]. Therefore, in some cases no hexagonal phase was found for samples doped even up to 2.5 mol% iron and prepared at 1400 °C in air, see e.g. [9–11] (ceramics) and [12] (single

[3] Author to whom any correspondence should be addressed.

crystals). In the 1980s Fe-doped $BaTiO_3$ became prominent because of its outstanding photorefractive properties [13, 14]. Since the necessary doping concentration for photorefractive applications is in the range of 0.1 mol%, the Fe-doped samples remain tetragonal at RT. A new promising application of iron doped $BaTiO_3$ was opened in 2001 by the finding of simultaneous ferroelectric and ferrimagnetic properties in thin films by Maier *et al* [15]. In the following years numerous papers on Fe-doped $BaTiO_3$ dealing with its potential multiferroic properties were published, see e.g. [2–4, 16–20]. While magnetic hysteresis loops were usually measured to prove the ferromagnetic properties of the samples, see e.g. [2, 16], systematic measurements of the magnetic susceptibility as functions of temperature and magnetic field in dependence on the Fe content for low concentrations $\leqslant$5 mol% are scarce [2, 19]. Several explanations of the observed ferromagnetism are discussed in literature. For example, Lin *et al* [16] considered the ferromagnetism of Fe doped $BaTiO_3$ as an intrinsic property originating from superexchange interactions between Fe^{3+} in different occupational sites associated with oxygen vacancies. Several authors suspected additional antiferromagnetic (AFM) interactions between the Fe ions, but without direct experimental evidence. Only Barbier *et al* reported on AFM spin-ordering detected by x-ray magnetic absorption circular dichroic (XMCD) measurements in Fe-doped multiferroic $BaTiO_3$ thin films [21].

To understand the magnetic properties of hexagonal 6H-$BaTiO_3$, detailed knowledge about the incorporation site of paramagnetic Fe ions in the lattice and their interaction with oxygen vacancies is of fundamental importance. By means of local-probe measurements, such as electron paramagnetic resonance (EPR) on single crystals, the nature of such iron centers can be studied comprehensively. In our previous paper [7], we presented EPR investigations of single crystal and ceramic Fe doped hexagonal $BaTiO_3$ giving detailed microscopic information on the iron defects. We found isolated Fe^{3+} located both at Ti(1) and Ti(2) sites and one Fe^{3+}–V_O associate. The labeling of the atoms follows Burbank and Evans [22]. The Ti(1) site refers to the 2a position (0, 0, 0) belonging to exclusively corner-sharing oxygen octahedra, while Ti(2) refers to the 4f position (1/3, 2/3, 0.154) belonging to the Ti_2O_9 units of two face-sharing oxygen octahedra in the 6H-structure (space group $P6_3/mmc$). The face-sharing oxygen ions are denoted by O(1) and the others by O(2).

In the present paper we extent the investigations of the effect of iron on the magnetic properties of hexagonal barium titanate by systematic measurements of the magnetic moment in dependence on temperature and magnetic field strength in the concentration range between 0.5 and 5.0 mol% Fe. These measurements provide clear evidence of Fe–Fe interactions which is further supported by EPR measurements.

Optical transmission measurements can yield additional information about the position of the defect levels in the band gap. Since no optical transmission data of hexagonal 6H-$BaTiO_3$ were published yet, we present such data in the visible and near UV range and compare the results with corresponding data of the tetragonal 3C modification of $BaTiO_3$ [12].

Additionally, the paper presents Q-band EPR measurements on single crystals doped with 5.0 mol% Fe. These investigations were done to verify the position of the earlier detected Fe^{3+}–V_O associate [7]. Theoretical investigations [23, 24] predict the associate $Fe^{3+}_{Ti(2)}$–$V_{O(1)}$ to be most stable, in which the oxygen vacancy is located in the O(1) plane connecting the face-sharing oxygen octahedra. In contrast, our EPR data exclude the formation of this defect.

2. Experimental procedure

Ceramic powders with the nominal composition $BaTiO_3$ + 0.04 BaO + 1/2 x Fe_2O_3 ($0.005 \leqslant x \leqslant 0.05$) were prepared by the conventional mixed-oxide powder technique. After mixing (agate balls, water) and calcining (1100 °C, 2 h) of $BaCO_3$ (Solvay, VL600, <0.1 mol% Sr) and TiO_2 (Merck, no. 808), Fe_2O_3 (Merck, p.a.) was added to the obtained $BaTiO_3$ powder. Afterwards, the mixture was fine-milled (agate balls, 2-propanole) and pressed to disks with a diameter of 6 mm and a height of approximately 3 mm. The samples were sintered in air at 1400 °C for 1 h (heating rate 10 K min^{-1}).

Magnetic measurements were carried out using the ACMS magnetometer option of a PPMS 9 (Quantum Design). The temperature-dependent magnetic moments were measured up to 9.0 T in the temperature range 5–300 K using field-cooled (FC) and zero-field-cooled (ZFC) conditions. The obtained magnetic moments were corrected for the magnetic moment of the sample holder and with respect to the magnetic contribution of the $BaTiO_3$ matrix.

Room temperature optical absorption measurements in the 350–800 nm region were performed using a microscope photometer model MPM 800D/UV (Carl Zeiss, Germany). To achieve sufficient optical transmission the samples were thinned down to a thickness below 15 μm by mechanical grinding and polishing. The instrument allows measuring areas down to 5 $\times$ 5 μm^2, enabling the investigation of single, homogeneous grains of the ceramics, which corresponds to investigations of single crystalline samples.

Single crystals with nominal composition $BaTi_{0.95}Fe_{0.05}O_3$ were grown by a floating zone method. Details are described in [7]. EPR measurements of the single crystals were carried out in the Q-band with a Bruker spectrometer (for details see [7]).

3. Results and discussion

3.1. Magnetic measurements

3.1.1. High magnetic field. The temperature dependent molar magnetic susceptibilities χ_{mol} of the samples in the concentration range between 0.5 and 5.0 mol% are shown in figure 1. All samples were as-sintered in air and measured in a magnetic field of 9.0 T. The obtained data was normalized to the nominal Fe content (x). Interestingly, the susceptibility of the samples with low Fe content, namely of 0.5, 0.7 and 1.0 mol% exhibit equal values whereas the susceptibility of the samples with an increased Fe content of 2.0 and 5.0 mol% decrease with rising Fe content. This behavior is better visible in the $n_{eff}(T)$ plot [25, 26] shown as the right scale

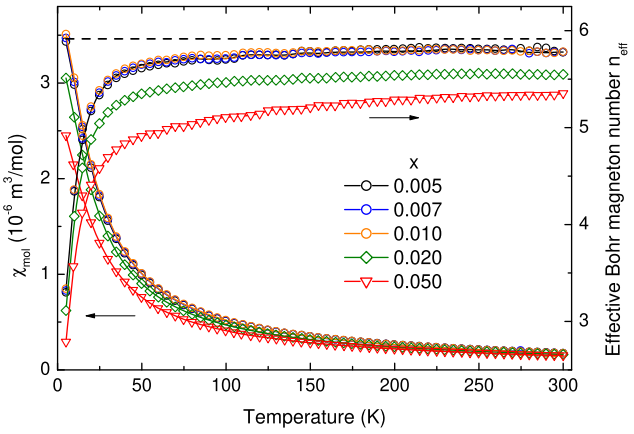

Figure 1. Temperature dependence of molar magnetic susceptibilities and effective Bohr magnetons of Fe-doped hexagonal $BaTiO_3$ ceramics with different iron mole fractions x measured at a magnetic field of 9.0 T. The spin-only-value of n_{eff} for high-spin Fe^{3+} ($S = 5/2$) is plotted as a dashed line.

in figure 1. The effective number n_{eff} of Bohr magnetons μ_{B} of the paramagnetic ion is defined as

$$n_{\mathrm{eff}} = \sqrt{\frac{3k_{\mathrm{B}}\chi_{\mathrm{mol}}\,T}{\mu_0 N_{\mathrm{A}}\mu_{\mathrm{B}}^2}} \qquad (1)$$

(k_{B}—Boltzmann constant, μ_0—permeability of vacuum, N_{A}—Avogadro constant).

The high spin $3d^5$ electron configuration ($S = 5/2$) with its ground term $^6A_{1g}$ (resulting from the free ion term ^6S in an octahedral crystal field) is one case of the good validity of the spin-only approach $n_{\mathrm{eff}} = 2\sqrt{S(S+1)}$ [24]. This value (=5.92, shown as straight line in figure 1) corresponds well with the n_{eff} data of the samples with [Fe] $\leqslant$ 1.0 mol% for $T > 100$ K, confirming the presence of isolated Fe^{3+} ions (high spin d^5) in hexagonal $BaTiO_3$ [7]. It proves that the magnetic susceptibility of these samples is mainly caused by isolated paramagnetic iron defects. The decreased molar susceptibility of the samples with higher Fe concentration points to an additional effect related to the Fe^{3+} ions, which is assumed as an antiferromagnetic ordering of Fe^{3+} pairs (dimer coupling) by exchange interaction [27, 28] reducing the total magnetic moment of the samples. The exchange can be realized either by direct interaction of Fe^{3+} ions at neighboring Ti(2) sites due to their small distance of 2.75 Å [29] or by superexchange via an intervening O(2) ion [30]. Hence, the total magnetic molar susceptibility of the samples with 2.0 and 5.0 mol% Fe can be described by a superposition of a paramagnetic (PM) and an antiferromagnetic (AFM) contribution according

$$\chi_{\mathrm{mol}}^{\mathrm{tot}} = (1 - \mathrm{w})\,\chi_{\mathrm{mol}}^{\mathrm{PM}} + \mathrm{w}\,\chi_{\mathrm{mol}}^{\mathrm{AFM}}. \qquad (2)$$

The weighting factor w of the AFM portion was determined by fitting of the measuring data with the program CONCORD [31] using the ligand field approach. Details of the program can be found e.g. in [32]. The contribution $\chi_{\mathrm{mol}}^{\mathrm{PM}}$ was obtained from a fit of the data of the sample with $x = 0.007$ again by CONCORD with the octahedral crystal field parameter B40 (Wybourne notation [33]) as the refined parameter. An

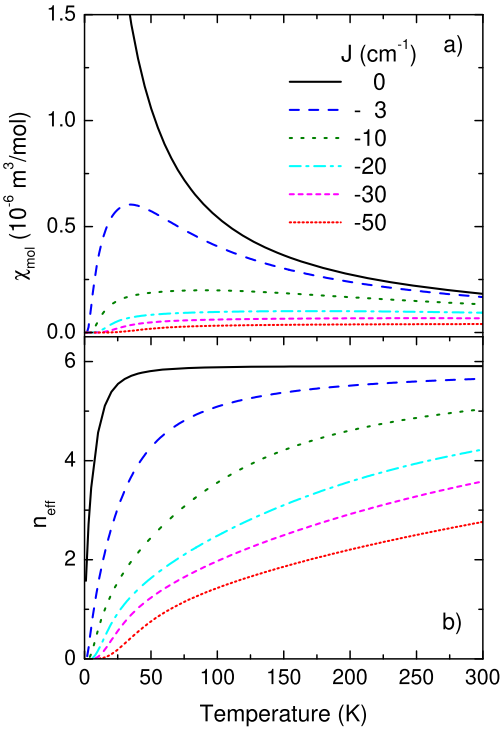

Figure 2. Simulated temperature dependent molar magnetic susceptibilities and effective Bohr magnetons of Fe^{3+} dimers for different values of the Heisenberg coupling parameter J.

excellent description of the experimental data was achieved with the parameters B40 = 44 000 cm^{-1} and fixed single electron spin–orbit coupling parameter $\zeta = 400$ cm^{-1} and orbital reduction parameter $\kappa = 1.0$. With these parameters the AFM contribution was simulated in the next step assuming a Heisenberg coupling and applying different exchange constants $J = -3, -10, -20, -30, -50$ cm^{-1}. Results are shown in figure 2 together with the calculated values of n_{eff}. Compared to the isolated Fe^{3+} ion ($J = 0$), χ_{mol} and n_{eff} decrease with increasing AFM interaction strength $|J|$ as expected. The molar magnetic susceptibilities of the samples with 2.0 and 5.0 mol% were fitted for all five values of J (see figure 2) and the results are listed in table 1. The best fit according to the minimum of the square root of the so-called χ^2/dof value (dof = degree of freedom) was reached for $J = -10$ cm^{-1} and $J = -20$ cm^{-1} for the samples with 2.0 mol% and 5.0 mol% iron, respectively. Figure 3 shows the very good agreement between the experimental data and the fitting curves. With these values the AFM portion of the samples with 2.0 mol% and 5.0 mol% Fe amounts to about 0.12 and 0.29. As seen in table 1, the results for w show only a small dependence on J and are therefore quite stable. It can therefore be concluded that for $x = 0.02$ about 12% of the iron ions form antiferromagnetic coupled dimers, whereas the portion of dimers increase to roughly 30% for $x = 0.05$.

The nature of the AFM coupling mechanism (direct or superexchange) cannot be derived from our magnetic measurements. In literature, AFM interactions between transition metal dopants in oxides are mostly discussed as a super exchange mechanism via an oxygen ion [27, 34, 35], because of an insufficient direct overlap between neighboring magnetic orbitals of the metal ions. As pointed out above, the

Table 1. Fit results of $\chi_{\mathrm{mol}}(T)$ at 9.0 T with the model function according equation (2) for the samples with $x = 0.02$ und 0.05. RMSD is the root-mean-square deviation of the experimental and calculated values. Bold marked values are the best fits (lowest RMSD).

J (cm^{-1})	$x = 0.02$		$x = 0.05$	
	w	RMSD (10^{-8} m^3 mol^{-1})	w	RMSD (10^{-8} m^3 mol^{-1})
−3	0.146	2.85	0.357	6.62
−9	0.126	1.08		
−10	**0.125**	**0.99**	0.307	1.64
−20	0.119	1.02	**0.293**	**1.17**
−30	0.116	1.26	0.287	1.82
−50	0.114	1.50	0.283	2.49

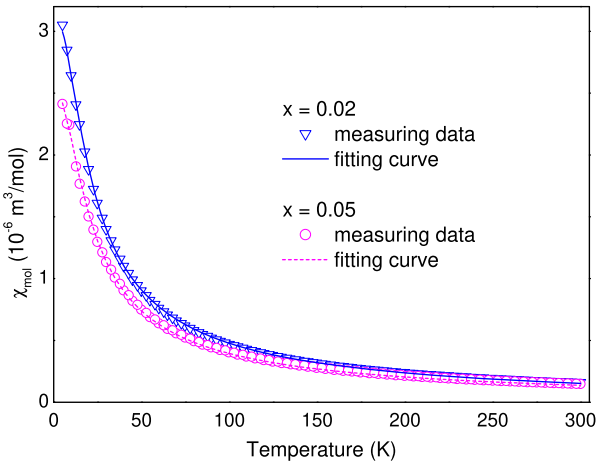

Figure 3. Experimental data and fit results for the molar magnetic susceptibility of the samples with 2.0 mol% and 5.0 mol% Fe measured at $B = 9.0$ T.

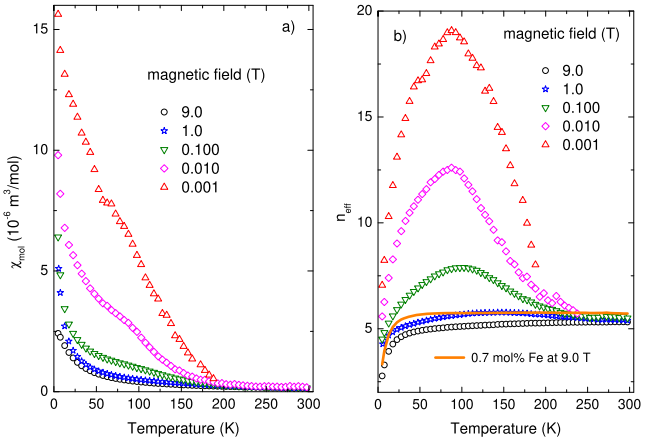

Figure 4. Temperature-dependent molar magnetic susceptibilities (a) and effective Bohr magnetons (b) of the sample with 5.0 mol% Fe for different magnetic fields between 9 T and 1 mT. For the lowest magnetic field of 1 mT the measured magnetic moments above 200 K are in the range of the absolute measuring sensitivity of the PPMS and were therefore omitted.

shortest Fe–Fe distance between the centers of the face-sharing octahedra (neighboring Ti(2) sites) accounts to approximately 2.75 Å. Probably, this distance is too large for a direct exchange interaction strong enough to explain the AFM coupling of the samples with 2.0 and 5.0 mol% Fe, see page 273f of reference [35] and page 76 of reference [27]. Therefore, a super exchange mechanism seems more plausible. Another argument for the presence of an indirect AFM interaction arises from the different probabilities of the occurrence of configurations with direct ($Fe_{Ti(2)}$–$Fe_{Ti(2)}$) or indirect ($Fe_{Ti(1)}$–O(2)–$Fe_{Ti(2)}$) exchange. Whereas a given Ti(2) site has only one direct Ti(2) neighbor, it has three Ti(1) neighbors and a given Ti(1) site has even six Ti(2) neighbors. Hence, assuming a random distribution of the Fe atoms on both different Ti sites, the relative probability of a configuration with direct interaction is less than 25% of the probability of a configuration with indirect interaction.

3.1.2. Variation of the magnetic field strength. It is well-known that strong magnetic fields may affect considerably the susceptibility data leading to magnetic saturation and distortion of weak electronic couplings [26]. Therefore, measurements of the molar magnetic susceptibility were performed at different magnetic fields of 9.0 T, 1.0 T, 100mT, 10 mT and 1 mT. Figure 4(a) shows the results for the sample with the highest iron content of 5.0 mol%. The samples with lower Fe contents show a similar behavior but the effects discussed in the following become smaller with decreasing Fe content and therefore they are not shown.

With decreasing magnetic field, χ_{mol} increases systematically and for $B \leqslant 0.1$ T distinct deviations from the Curie–Weiss behavior appear below 200 K. Again, the effective Bohr magneton number n_{eff} shown in figure 4(b) provides a clearer picture of this effect. Since the susceptibility and n_{eff} values for $B \leqslant 0.1$ T exceed the ones for pure paramagnetism (shown for the sample with $x = 0.007$ for n_{eff} in figure 4(b)), this effect points to a ferromagnetic coupling. For $B \leqslant 0.1$ T the $n_{\mathrm{eff}}(T)$ curves exhibit a distinct maximum at roughly 90 K.

Hence, the total magnetic moment of the samples can be described as a superposition of three contributions, namely the paramagnetic, an antiferromagnetic and a ferromagnetic component. The contributions of these effects depend on the Fe concentration and on the applied magnetic field.

The total molar magnetic susceptibility can be written as

$$\chi_{\mathrm{mol}}^{\mathrm{tot}} = \chi_{\mathrm{mol}}^{\mathrm{PM}} + \chi_{\mathrm{mol}}^{\mathrm{AFM}} + \chi_{\mathrm{mol}}^{\mathrm{FM}} \qquad (3)$$

Under the assumption that the ratio between the PM and AFM contribution does not depend on the magnetic field, the

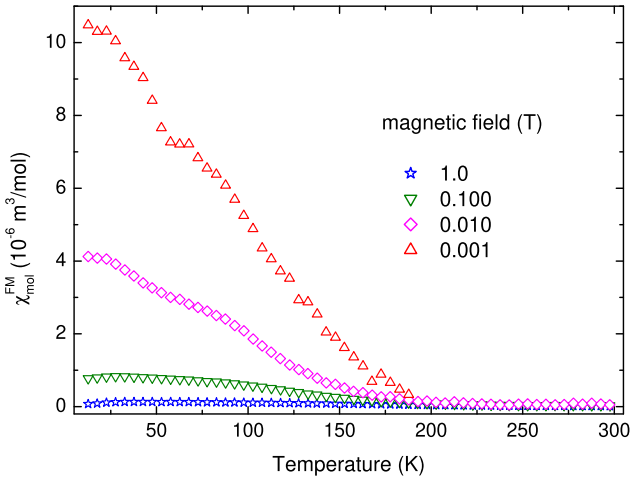

Figure 5. Ferromagnetic contribution to the molar magnetic susceptibility for different magnetic fields strengths between 1 mT and 1.0 T of the sample doped with 5.0 mol% Fe. See text for details.

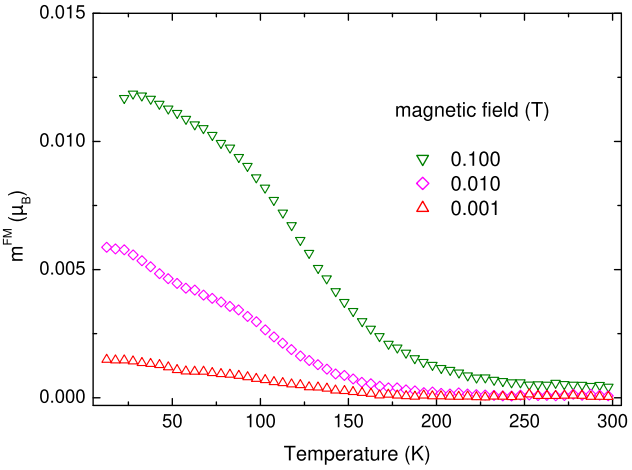

Figure 6. Average magnetic moment of the FM Fe^{3+} clusters for different magnetic fields between 1 mT and 100 mT calculated with respect to the total Fe content for the sample doped with 5.0 mol% Fe.

FM portion of the sample with 5.0 mol% Fe can be calculated as

$$\chi^{\mathrm{FM}}_{\mathrm{mol}}(B) = \chi^{\mathrm{tot}}_{\mathrm{mol}}(B) - 0.71\chi^{\mathrm{PM}}_{\mathrm{mol}}(B) - 0.29\chi^{\mathrm{AFM}}_{\mathrm{mol}}(B) \quad (4)$$

using the estimated ratio between $\chi^{\mathrm{PM}}_{\mathrm{mol}}$ and $\chi^{\mathrm{AFM}}_{\mathrm{mol}}$ at $B = 9.0$ T (see section 3.1.1). The field-dependent PM and AFM contributions were calculated by CONCORD with the parameters given above and an AFM exchange constant of $J = -20\ \mathrm{cm}^{-1}$.

The obtained ferromagnetic contributions to the total magnetic susceptibility are shown in figure 5 for the different magnetic fields. The magnetic moment of the Fe^{3+} clusters probably causing the ferromagnetic effect was calculated based on the total concentration of Fe^{3+} ions in the sample according

$$m^{\mathrm{FM}} = \frac{\chi^{\mathrm{FM}}_{\mathrm{mol}} H}{N_{\mathrm{A}}}. \quad (5)$$

This procedure most likely strongly underestimates the real value of the magnetic moment of the Fe^{3+} clusters, whose concentration is unknown. The obtained values are presented for the magnetic fields between 0.001 T and 0.1 T in figure 6. The onset of the FM effect below 200 K (see figure 4(a)) is not well reflected in figure 6 due to the very small differences of the measured data at all applied magnetic fields for $T > 200$ K. For the same reason, the calculation of the curve for $B = 1.0$ T led to large uncertainties and is therefore not shown in figure 6.

Nevertheless, it can be stated that the magnetic moment of the FM species increases with the magnetic field indicating that there is still no saturation of the magnetic moment of the clusters until the strong magnetic field $\geqslant$1.0 T destroys this weak FM interaction.

The origin of the ferromagnetic interaction of Fe^{3+} ions can hardly be determined from the evaluation of the presented data. Because of the weakness of the FM interaction, which is suppressed both by sufficient high magnetic and thermal energies, here the direct exchange between Fe^{3+} ions at neighboring Ti(2) sites could come into play. But there are also reported weak FM interactions by a super exchange mechanism via an oxygen ligand if the metal–O–metal angle is nearly 90° [34, 35]. This geometry occurs in hexagonal $BaTiO_3$ where the $Fe^{3+}_{Ti(2)} - O(1) - Fe^{3+}_{Ti(2)}$ angle is 85° (undoped $BaTiO_3$ [29]). Moreover, also clusters of more than two Fe^{3+} ions might exist in the hexagonal $BaTiO_3$ structure with oxygen vacancies involved.

The presence of AFM and FM interactions between neighboring Fe^{3+} ions discussed can explain the presence of several additional weak lines in the EPR Q-band spectra in single crystalline samples with 2.0 and 5.0 mol% Fe, which cannot be related to the defects identified in our recent paper [7]. Their intensities depend on the Fe-concentration, and are about 1.6 times larger in the crystal with 5.0 mol% Fe in comparison to sample with 2.0 mol% Fe. For the orientation of the crystal close to $B \parallel$ c up to 22 lines appear in the spectrum (see figure 7). These lines show a strong angular dependence. We assume that these EPR lines are caused by interactions between different Fe^{3+}_{Ti} ions, since the number of randomly neighboring Fe^{3+} ions increases with increasing Fe concentration. On the other hand, a comprehensive analysis is not possible because of the complexity of the very weak spectrum, the strong angular dependence of the lines and the severe overlapping with the much stronger Fe^{3+}-lines marked in figure 7.

3.2. Optical transmission

It is known from literature that Fe impurities cause an apparent decrease of the optical band gap of the tetragonal 3C-$BaTiO_3$ single crystals obtained from different crystal growth methods [12]. Here, we present the results of optical transmission measurements on single grains of thinned ceramic samples of the hexagonal 6H modification sintered at 1400 °C. Figure 8 shows the absorbance in the range between 350 and 750 nm of a sample doped with 2.0 mol% Fe in comparison with an undoped specimen. A shift of the absorption edge by about 0.3 eV upon iron doping is clearly visible. The absorbance is

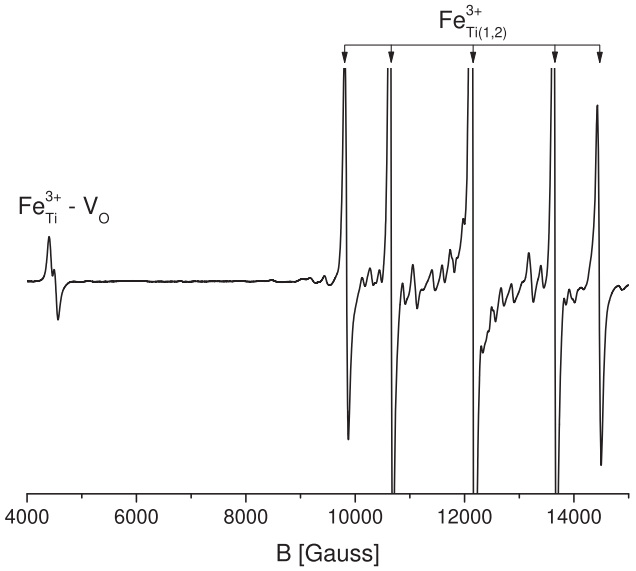

Figure 7. Room temperature Q-band spectrum of a hexagonal $BaTiO_3$ single crystal doped with 5.0 mol% Fe. The direction of the magnetic field is parallel to the crystallographic *c* axis.

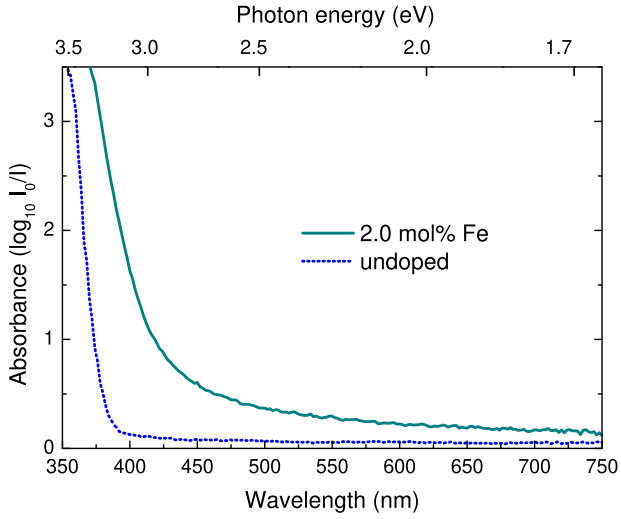

Figure 8. Room temperature optical transmission spectra in the UV/Vis range of an undoped and a 2.0 mol% Fe-doped hexagonal $BaTiO_3$ sample.

rather high, therefore it seems unlikely that it is caused by a d–d transition, which is spin-forbidden in high-spin Fe^{3+} ($t_{2g}{}^3e_g{}^2$). The observed optical transition is more likely caused either by a transition

$$Fe^{3+} \rightarrow Fe^{4+} + 1e\ (\text{conduction band})$$

with a defect level in the band gap near the valence band edge, or by a charge transfer transition

$$Fe^{3+} + 1e\ (\text{valence band}) \rightarrow Fe^{2+}$$

with a defect level near the conduction band edge [34]. The transition

$$Fe^{4+} + 1e\ (\text{valence band}) \rightarrow Fe^{3+}$$

can be ruled out, since the magnetic measurements brought no indication of significant concentration of Fe^{4+} ions in the samples. According to the literature, the charge transfer transition is more probable [13]. Unfortunately, both the Fe^{2+} and Fe^{4+} defects are EPR silent. Therefore, EPR measurements under illumination with UV light did not lead to any additional lines. Neither did the EPR intensity of the Fe^{3+} centers change significantly. A very recent work on first-principles calculations by density functional theory of 2 mol% Fe-doped hexagonal $BaTiO_3$ [24] showed clear evidence for a strong partial density of states of Fe^{3+} in the band gap both near the valence band (Fe^{3+} at Ti(2) site) and the conduction band (Fe^{3+} at Ti(1) site). Therefore both electron transitions discussed above seem to be possible.

3.3. Q-band EPR investigations on 6H-$BaTiO_3$ single crystals

Our previous X-band EPR investigations on single crystals [7] were extended to Q-band measurements on a sample with 5.0 mol% Fe. The reason for the additional Q-band EPR investigation is the improved separation of the spectra of the isolated Fe^{3+} centers ($Fe^{3+}_{Ti(1)}$ and $Fe^{3+}_{Ti(2)}$) from the one of the associate centers Fe^{3+}–V_O as a consequence of the large difference in the fine structure tensors (figure 7). Because of the two different Ti-sites in the 6H-$BaTiO_3$ lattice there are several possibilities for the formation of such associate centers. If the exclusively corner-sharing octahedron is affected, the oxygen vacancy can be located at each of the six O(2) sites surrounding the Ti(1) site. Because the six $Fe^{3+}_{Ti(1)}$–$V_{O(2)}$ distances are equal (and therefore also the total electrical field at the Fe site in the differently oriented associate centers), only one kind of associate centers (type 1) is expected. On the basis of the various orientations of this $Fe^{3+}_{Ti(1)}$–$V_{O(2)}$ associate with respect to the crystal axes, type 1 generates several sets of EPR spectra in single-crystal experiments. However, the number of sets is reduced to three by the crystal symmetry. Therefore, upon rotating the crystal around the hexagonal *c*-axis three spectra are observed which transform into one another by a $\pi/3$-rotation.

The location of the Fe^{3+}–V_O associate in the face-sharing octahedra causes a more complex situation. In this case, two different O–Ti distances exist due to the local 3*m* symmetry of the 4f position: three shorter distances $R_{Ti(2)-O(2)} = 1.958$ Å and three larger ones $R_{Ti(2)-O(1)} = 1.992$ Å.[4] Therefore, two kinds of Fe^{3+}–V_O associates (types 2 and 3) are expected and the fine structure tensors for the two types should differ. The EPR spectra of type 2 and type 3 have the same symmetry properties with respect to the rotation pattern as that of type 1, i.e. three sets for each type are expected in the *c*-rotation pattern so that an assignment to the different types based on the line numbers is not possible. If structurally different Fe^{3+}–V_O centers with similar fine structure tensors are present in the crystals, line splitting effects should be easier detectable in the Q-band spectra than in those in X-band. In our previous X-band investigations on 2.0 mol% Fe doped crystals only one

[4] Data from undoped hexagonal 6H-$BaTiO_3$ [29].

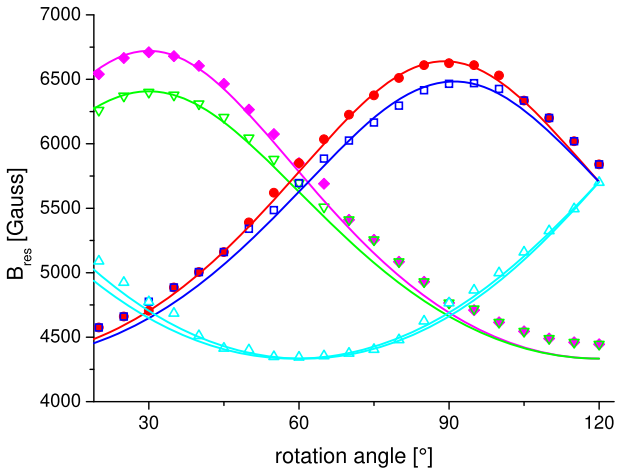

Figure 9. Angular dependence of the Fe^{3+}–V_O resonance fields (shown as symbols) in the room temperature Q-band spectra of a hexagonal $BaTiO_3$ single crystal doped with 5.0 mol% Fe. The crystal was rotated approximately around the *c*-axis; rotation angle of 90° corresponds to $B \parallel$ b. The fitting curves (solid lines) were calculated using the parameters given in tables 1 and 2 of [3].

kind of Fe^{3+}–V_O associate centers could be detected. Thus, we performed additional Q-band measurements to identify possible other types of associate centers in the higher doped crystal with 5.0 mol%, which cannot be excluded *a priori*.

As shown in figure 7, besides the spectra of the isolated Fe centers ($Fe^{3+}_{Ti(1)}$ and $Fe^{3+}_{Ti(2)}$), several lines in the magnetic field range around 4500 Gauss were observed, which are assigned to associate centers (figure 7). In figure 9 the rotation pattern of the resonance fields for strongly angle-dependent lines upon rotation around the *c*-axis is depicted. The angular dependence of the resonance fields was simulated using the experimentally determined spin-Hamiltonian parameters obtained in our earlier X-band investigations (cf tables 1 and 2 in [7]) and the results are shown as curves in figure 9. The experimentally observed larger number of resonances indicates a slight misalignment of the crystal by approximately 3°. A small misorientation was in fact verified by single crystal XRD measurements and accounted to 2.7°. Therefore, during the EPR investigations the crystal was in fact rotated around [0.0 0.021 1.0]. Because this axis is no symmetry axis of the hexagonal crystal the magnetic equivalence of the differently oriented Fe–V_O centers of this type is broken and consequently more lines appear in the rotation pattern in comparison to the [001] pattern as shown in figure 6 of our previous paper [7]. Apart from the doubling of the known associate center due to the misalignment no additional resonances were observed. Hence, probably only one of the three types of associate centers discussed above occurs in the samples with 2.0 and also with 5.0 mol% Fe. Since no further type of Fe–V_O centers were detected in the Q-band spectra it can be concluded that the oxygen vacancies adjacent to the Fe^{3+} ions are located on O(2)-sites in the exclusively corner- or face-sharing octahedra [7].

4. Conclusions

Systematic investigations of the magnetic properties of iron-doped ceramic hexagonal $BaTiO_3$ samples revealed three different types of magnetic behavior dependent on Fe content and strength of the external magnetic field. While for Fe concentrations $\leqslant$1.0 mol% the temperature-dependent magnetic susceptibilities can be very well described by a Curie behavior, samples with 2.0 mol% and 5.0 mol% Fe exhibit AFM interaction between Fe^{3+} ions whose contribution increases with rising Fe content. Below 1.0 T, a third effect: weak ferromagnetism is detected for the samples with higher Fe concentrations. The ferromagnetic interaction of the Fe^{3+} ions is totally suppressed by a magnetic field of 9.0 T and vanishes at temperatures >200 K. These Fe^{3+}–Fe^{3+} interactions are also manifest in EPR Q-band spectra of single crystals with 2.0 mol% and 5.0 mol% as very numerous low-intensity lines.

The angular dependence of the resonance fields in room temperature EPR Q-band spectra of a 5.0 mol% Fe doped single crystal upon rotation around the *c*-axis strengthens the finding of our previous paper [7] (based on X-band measurements on a 2.0 mol% Fe doped single crystal) that only one type of associates between Fe^{3+} and oxygen vacancies occur, namely the complex $Fe^{3+}_{Ti(1)}$–$V_{O(2)}$.

Acknowledgments

The authors thank Christine Seidel (Institute of Chemistry, Faculty of Natural Sciences II, Martin-Luther-Universität Halle-Wittenberg) for the measurement of the optical absorption including the careful preparation of thinned ceramic samples.

ORCID iDs

H T Langhammer https://orcid.org/0000-0003-2603-093X
S G Ebbinghaus https://orcid.org/0000-0001-6391-2582

References

[1] Coey J M D 2006 *Curr. Opin. Solid State Mater. Sci.* **10** 83
[2] Ray S, Mahadevan P, Mandal S, Krishnakumar S R, Kuroda C S, Sasaki T, Taniyama T and Itoh M 2008 *Phys. Rev.* B **77** 104416
[3] Chakraborty T, Ray S and Itoh M 2011 *Phys. Rev.* B **83** 144407
[4] Valant M, Arčon I, Mikulska I and Lisjak D 2013 *Chem. Mater.* **25** 3544
[5] Glaister R M and Kay H F 1960 *Proc. Phys. Soc.* **76** 763
[6] Böttcher R, Langhammer H T, Müller T and Abicht H-P 2008 *J. Phys.: Condens. Matter.* **20** 505209
[7] Böttcher R, Langhammer H T, Kücker S, Eisenschmidt C and Ebbinghaus S G 2018 *J. Phys.: Condens. Matter.* **30** 425701
[8] Langhammer H T, Müller T, Felgner K-H and Abicht H-P 2000 *Mat. Lett.* **42** 21
[9] Hagemann H-J and Ihrig H 1979 *Phys. Rev.* B **20** 3871
[10] Hagemann H-J, Hero A and Gonser U 1980 *Phys. Status Solidi a* **61** 63
[11] Hagemann H-J and Hennings D 1981 *J. Am. Ceram. Soc.* **64** 590
[12] Godefroy G, Dumas C, Lompré P and Perrot A 1981 *Ferroelectrics* **37** 725
[13] Klein M B 1988 *Photorefractive Properties of BaTiO3 Chapter 7 of Photorefractive Materials and Their Applications I* (Topics in Applied Physics vol 61) (Berlin: Springer)

[14] Briat B, Grachev V G, Malovichko G I, Schirmer O F and Wöhlecke M 2007 *Defects in Inorganic Photorefractive Materials and Their Investigations Chapter 2 of Photorefractive Materials and Their Applications II* (New York: Springer)
[15] Maier R, Cohn J L, Neumeier J J and Bendersky L A 2001 *Appl. Phys. Lett.* **78** 2536
[16] Lin F, Jiang D, Ma X and Shi W 2008 *J. Magn. Magn. Mater.* **320** 691
[17] Xu B, Yin K B, Lin J, Xia Y D, Wan X G, Yin J, Bai X J, Du J and Liu Z G 2009 *Phys. Rev.* B **79** 134109
[18] Zorko A, Pregelj M, Gomilšek M, Jagličić Z, Pajić D, Telling M, Arčon I, Mikulska I and Valant M 2015 *Sci. Rep.* **5** 7703
[19] Deka B and Ravi S 2018 *J. Supercond. Nov. Magn.* **31** 1427
[20] Pal P *et al* 2020 *Phys. Rev.* B **101** 064409
[21] Barbier A *et al* 2015 *Phys. Rev.* B **91** 035417
[22] Burbank R D and Evans H TJr 1948 *Acta Crystallogr.* **1** 330
[23] Dawson J A, Freeman C L, Harding J H and Sinclair D C 2013 *J. Solid State Chem.* **200** 310
[24] Adeagbo W A, Ben Hamed H, Nayak S K, Böttcher R, Langhammer H T and Hergert W 2019 *Phys. Rev.* B **100** 184108
[25] Lueken H 1999 *Magnetochemie* (Stuttgart: Teubner)
[26] Hatscher S, Schilder H, Lueken H and Urland W 2005 *Pure Appl. Chem.* **77** 497
[27] Blundell S 2001 *Magnetism in Condensed Matter* (Oxford: Oxford University Press)
[28] Craik D J 1998 *Magnetism: Principles and Applications* (Chichester: Wiley)
[29] Akimoto J, Gotoh Y and Oosawa Y 1994 *Acta Crystallogr.* C **50** 160
[30] Anderson P W 1959 *Phys. Rev.* **115** 2
[31] Schilder H 2015 Programm CONCORD, Fachhochschule Aachen http://condon.fh-aachen.de
[32] Langhammer H T, Böttcher R, Müller T, Walther T and Ebbinghaus S G 2015 *J. Phys.: Condens. Matter.* **27** 295901
[33] Wybourne B G 1965 *Spectroscopic Properties of Rare Earths* (New York: Wiley)
[34] Cox P A 1995 *Transition Metal Oxides* (Oxford: Clarendon)
[35] Figgis B N and Hitchman M A 2000 *Ligand Field Theory and its Applications* (New York: Wiley)